

1 **NeutrobodyPlex - Nanobodies to monitor a SARS-CoV-2 neutralizing immune response**

2

3 *Teresa R. Wagner^{1,2}, Philipp D. Kaiser², Marius Gramlich², Matthias Becker², Bjoern Traenkle²,*
4 *Daniel Junker², Julia Haering², Helen Schweizer³, Stefan Nueske³, Armin Scholz³, Anne Zeck²,*
5 *Katja Schenke-Layland^{2,4,6,7}, Annika Nelde^{8,9}, Monika Strengert^{11,12}, Gérard Krause^{11,12},*
6 *Juliane S. Walz^{4,8,9,10}, Natalia Ruetalo⁵, Michael Schindler⁵, Nicole Schneiderhan-Marra² and*
7 *Ulrich Rothbauer^{1,2#}*

8

9 Addresses

10 ¹ Pharmaceutical Biotechnology, Eberhard Karls University Tuebingen, Germany

11 ² Natural and Medical Sciences Institute at the University of Tuebingen, Germany

12 ³ Livestock Center of the Faculty of Veterinary Medicine, Ludwig Maximilians University
13 Munich, Oberschleissheim, Germany

14 ⁴ Cluster of Excellence iFIT (EXC2180) "Image-Guided and Functionally Instructed Tumor
15 Therapies", University of Tuebingen, Tuebingen, Germany

16 ⁵ Institute for Medical Virology and Epidemiology of Viral Diseases, University Hospital,
17 Tuebingen, Germany

18 ⁶ Department of Women's Health, Research Institute for Womens's Health, Eberhard-Karls-
19 University, Tuebingen, Germany

20 ⁷ Department of Medicine/Cardiology, Cardiovascular Research Laboratories, David Geffen
21 School of Medicine at UCLA, Los Angeles, CA, USA

22 ⁸ Clinical Collaboration Unit Translational Immunology, German Cancer Consortium (DKTK),
23 Department of Internal Medicine, University Hospital Tuebingen, Tuebingen, Germany

24 ⁹ Institute for Cell Biology, Department of Immunology, University of Tuebingen, Tuebingen,
25 Germany

26 ¹⁰ Department of Hematology, Oncology, Clinical Immunology and Rheumatology, University
27 Hospital Tuebingen, Tuebingen, Germany

28 ¹¹ Department of Epidemiology, Helmholtz Centre for Infection Research, Braunschweig,
29 Germany

30 ¹² TWINCORE GmbH, Centre for Experimental and Clinical Infection Research, a joint venture
31 of the Hannover Medical School and the Helmholtz Centre for Infection Research, Hannover,
32 Germany

33

34 # corresponding author

35

36 Correspondence:

37 Prof. Dr. Ulrich Rothbauer, Natural and Medical Sciences Institute at the University of
38 Tuebingen

39 Markwiesenstr. 55, 72770 Reutlingen, Germany.

40 E-mail: ulrich.rothbauer@uni-tuebingen.de

41 Phone: +49 7121 51530-415

42 Fax: +49 7121 51530-816

43 Ocid ID: 0000-0001-5923-8986

44

45 **Abstract**

46 Facing the worldwide disease progression of COVID-19 caused by the SARS-CoV-2 virus, the
47 situation is highly critical and there is an unmet need for effective vaccination, reliable diagnosis
48 and therapeutic intervention. Neutralizing binding molecules such as antibodies or derivatives
49 thereof have become important tools for acute treatment of COVID-19. Additionally, such
50 binders provide the unique possibility to monitor the emergence and presence of a neutralizing
51 immune response in infected or vaccinated individuals. Here we describe a set of 11 unique
52 nanobodies (Nbs), originated from an immunized alpaca which bind with high affinities to the
53 glycosylated SARS-CoV-2 Spike receptor domain (RBD). Using a multiplex *in vitro* binding
54 assay we showed that eight of the selected Nbs effectively block the interaction between RBD,
55 S1-domain and homotrimeric Spike protein with the angiotensin converting enzyme 2 (ACE2)
56 as the viral docking site on human cells. According to competitive binding analysis and detailed
57 epitope mapping, we grouped all Nbs blocking the RBD:ACE2 interaction in three distinct Nb-
58 Sets and demonstrated their neutralizing effect with IC_{50} values in the low nanomolar range in
59 a cell-based SARS-CoV-2 neutralization assay. Tested Nb combinations from different sets
60 showed substantially lower IC_{50} values in both functional assays indicating a profound
61 synergistic effect of Nbs simultaneously targeting different epitopes within the RBD. Finally,
62 we applied the most potent Nb combinations in a competitive multiplex binding assay which
63 we termed NeutrobodyPlex and detected a neutralizing immune response in plasma samples
64 of infected individuals. We envisage that our Nbs have a high potential for prophylactic as well
65 as therapeutic options and provide a novel approach to screen for a neutralizing immune
66 response in infected or vaccinated individuals thus helping to monitor the immune status or to
67 guide vaccine design.

68

69 **Introduction**

70 The pandemic of Corona Virus Disease 2019 (COVID-19) has been a tremendous wakeup call
71 as we are currently faced with a highly contagious virus that per mid-September 2020 has
72 caused the death of more than 900,000 people world-wide. Facing the current lack of cure or
73 approved vaccine most countries suffer from severe lockdowns and dramatic economic losses.
74 Neutralizing antibodies targeting the causative agent of the disease, the severe acute
75 respiratory syndrome coronavirus 2 (SARS-CoV-2), gain substantial interest for prophylactic
76 and therapeutic options and could help guide vaccine design [1]. These antibodies prevent
77 cellular entry by binding to the docking site of the virus. The SARS-CoV-2 virus binds to the
78 angiotensin converting enzyme II (ACE2) present on human lung epithelium via its receptor
79 binding domain (RBD) located within the homotrimeric transmembrane Spike glycoprotein
80 (Spike) forming a "large-area" interaction site [2]. Since the outbreak of the COVID-19
81 pandemic, a constantly growing number of neutralizing antibodies targeting the RBD of SARS-
82 CoV-2 has been identified from COVID-19 patients [1, 3] underlining the importance of RBD-
83 specific antibodies blocking the RBD:ACE2 interaction site for the development of a protective
84 immune response [4]. A promising alternative to conventional antibodies (IgGs) are single-
85 domain antibodies (nanobodies, Nbs) derived from the heavy-chain antibodies of camelids
86 **(Figure 1)**. Due to their small size and compact folding Nbs show a high chemical stability,
87 solubility and fast tissue penetration. Employing a targeted screening approach Nbs can be
88 selected against different epitopes on the same antigen and easily converted into multivalent
89 formats [5]. In comparison to antibodies Nbs have similar specificities and affinities and, due
90 to their high homology with human antibody (VH) fragments they show only very low
91 immunogenicity. With VHH-72 the first cross-reactive Nb which binds the RBD of SARS-CoV-
92 1 as well as of SARS-CoV-2 was recently reported [6]. Since this first publication, several
93 SARS-CoV-2 RBD specific Nbs were identified from naïve/ synthetic libraries [7-9] or
94 immunized animals [10-14]. However, to date only very few Nbs were identified displaying high
95 affinities in the monovalent format [8, 10]. Most of them have to be converted into multivalent
96 formats or applied as Fc fusion to efficiently block virus entry [6, 7]. This limits the developability

97 and applicability of those binders since protein size is distinctly increased and furthermore Fc
98 fusions bear the risk of unwanted antibody-dependent enhancement (ADE) in patients.
99 Additionally, the observed high mutation rate of SARS-CoV-2 [15, 16] further stresses the need
100 of selecting high affinity Nbs addressing multiple epitopes within the RBD to ensure sufficient
101 neutralization potency of virus harboring sequential and/ or structural changes in their docking
102 site.

103 Here we describe the selection of 11 unique Nbs, from a Nb gene library derived from an
104 alpaca immunized with glycosylated SARS-CoV-2 RBD. All Nbs can be readily produced in
105 bacteria at high yields and bind their target structure with strong affinities in their monovalent
106 format. Eight of the selected Nbs effectively block the interaction between RBD, S1-domain
107 and the homotrimeric Spike protein with ACE2 as the viral docking site in a multiplex *in vitro*
108 binding assay. Based on competitive binding analysis and detailed epitope mapping using
109 Hydrogen Deuterium Exchange mass spectrometry (HDX-MS) we clustered all ACE2 blocking
110 Nbs in three distinct Nb-Sets and demonstrated their potential to neutralize SARS-CoV-2
111 infection in a human cell model. By testing combinations from different Nb-Sets in both
112 functional assays, we achieved substantially improved IC₅₀ values indicating a highly
113 synergistic effect of Nbs targeting simultaneously different epitopes within the RBD. Finally,
114 we performed a competitive binding assay, which we termed NeurobodyPlex, using serum
115 samples from infected individuals and the most potent inhibitory Nb combinations. With this
116 approach we demonstrated the presence of antibodies in patient samples addressing the
117 RBD:ACE2 interface which are in accordance to previous findings designed as being
118 neutralizing antibodies. Based on the data presented here, we propose, that our Nbs have a
119 high potential for prophylactic and therapeutic options and provide a novel high-throughput
120 approach to screen for a neutralizing immune response in infected or vaccinated individuals
121 thus helping to monitor the immune status or to guide vaccine design.

122

123 **Results**

124 *Selection of Nbs binding to the RBD of SARS-CoV-2*

125 To generate Nbs directed against the RBD of SARS-CoV-2 we expressed and purified RBD in
126 mammalian (Expi293) cells [17] and immunized an alpaca (*Vicugna pacos*) following a 64-day
127 immunization protocol. Subsequently, we generated a Nb phagemid library comprising ~ 4 x
128 10⁷ clones representing the full repertoire of the variable heavy chains of heavy-chain
129 antibodies (V_HHs or Nbs) derived from the animal. The library was subjected to phage display
130 and biopanning was performed using either passively adsorbed or biotinylated RBD
131 immobilized on streptavidin plates. After two phage display cycles we analyzed 492 individual
132 clones in a solid-phase phage ELISA and identified 325 positive binders. Sequence analysis
133 of 72 clones revealed 11 unique Nbs which cluster in eight families with highly diverse
134 complementarity determining regions (CDR) 3 (**Figure 2 A**). Individual Nbs were cloned with
135 a C-terminal His₆-tag, expressed in *Escherichia coli* (*E.coli*) and purified using immobilized
136 metal ion affinity chromatography (IMAC) followed by size exclusion chromatography (SEC)
137 (**Figure 2 B**). For affinity measurements, we used biolayer interferometry (BLI) and
138 immobilized biotinylated RBD on the sensor tip. Incubation with serial dilutions of the Nbs
139 revealed K_D values ranging from ~1.3 nM to ~53 nM indicating a strong binding of the Nbs in
140 their monovalent format. NM1225 revealed a binding affinity in the micromolar range and was
141 therefore not considered for further analysis. (**Figure 2 C, Supplementary Figure 1**).

142

143 *Nbs compete with ACE2 for binding to RBD, S1 or homotrimeric Spike*

144 Next we analyzed the potential of the Nbs to block the interaction between homotrimeric Spike,
145 S1 domain or the RBD to ACE2. We utilized an in-house developed multiplex binding assay
146 for which we first covalently coupled the respective SARS-CoV-2 derived proteins on spectrally
147 distinct populations of paramagnetic beads (MagPlex Microspheres) [18]. For parallelized
148 analysis these beads were pooled and simultaneously incubated with biotinylated ACE2 and
149 dilutions of purified Nbs ranging from 2 μM to 12.3 pM. To screen for inhibitory Nbs, residual
150 binding of ACE2 to distinct viral antigens was detected on a Luminex instrument using R-

151 phycoerythrin (PE)-labeled streptavidin after stringent washing. Additionally, as negative
152 control a non-specific Nb (GFP-Nb) and as positive control two inhibiting mouse antibodies
153 were analyzed [19]. Data obtained by this multiplex binding assay showed that eight of the 10
154 analyzed Nbs inhibit ACE2 binding to isolated RBD, S1 domain and homotrimeric Spike. IC₅₀
155 values calculated for inhibition of ACE2:RBD interaction ranges between 0.5 nM for NM1228
156 and 38 nM for NM1229 (**Figure 3**). Notably, IC₅₀ values obtained for the most potent inhibitory
157 Nbs NM1228 (0.5 nM), NM1226 (0.85 nM) and NM1230 (2.12 nM) are highly comparable to
158 IC₅₀ values measured for the mouse IgGs (40591-MM43: 0.38 nM; 40592-MM57: 3.22 nM).
159 Additionally, the assay revealed that all Nbs except NM1224, show a similarly strong inhibitory
160 effect of ACE2 binding to all tested antigens. NM1224 seems to exclusively inhibit RBD:ACE2
161 interaction and does not prevent binding of ACE2 to neither homotrimeric Spike nor S1 domain.
162

163 *Epitope binning*

164 After identifying RBD-specific Nbs with inhibitory effect on ACE2 binding, we investigated the
165 relative location of their epitopes within the RBD. Thus, we first performed epitope binning
166 experiments of Nb combinations using BLI. After coating sensors with biotinylated RBD, a first
167 Nb was loaded until binding saturation was reached, followed by a short dissociation step to
168 remove excess Nb. A second Nb from a different family was then exposed to the RBD-Nb-
169 complex. Using this approach, we identified Nbs which recognize overlapping and non-
170 overlapping epitopes on RBD (**Figure 4, Supplementary Figure 2**). As expected Nbs with
171 only minor differences in their CDR3 (NM1221, NM1222 and NM1230, Nb-Set 2) were
172 suggested to recognize an identical or highly similar epitope as they cannot bind
173 simultaneously to RBD. Interestingly, our analysis revealed that Nbs with highly diverse CDR3s
174 such as NM1228, NM1226, NM1227 and NM1229 also could not bind simultaneously,
175 suggesting that these Nbs recognize similar or at least overlapping epitopes. Accordingly, we
176 clustered these diverse Nbs in Nb-Set 1. In total, based on epitope binning, we identified five
177 distinct Nbs-Sets, comprising at least one candidate targeting a different epitope within the
178 RBD compared to any member of a different Nb-Set (**Figure 4**).

179

180 *Epitope mapping of RBD binding Nbs*

181 We next performed Hydrogen-Deuterium Exchange Mass Spectrometry (HDX-MS) with the
182 most potent inhibitory Nbs selected from the different Nb-Sets to more precisely locate their
183 binding sites at the surface of RBD, and allowing comparison with the RBD:ACE2 interface.
184 Both members of Nb-Set1, NM1226 and NM1228, interacted with the RBD at the back/ lower
185 right site (Back View, **Figure 5**). Notably, the binding site of NM1226 does not encompass
186 amino acid residues involved in the RBD:ACE2 interface. In contrast, NM1228 (Nb-Set1) as
187 well as NM1230 (Nb-Set2) contacted RBD at amino acid residues overlapping with the
188 RBD:ACE2 binding interface, whereas NM1230 additionally covers parts of the spike-like loop
189 region on one edge of the ACE2 interface at the top front/ lower left side (Front View, **Figure**
190 **5**). In accordance to our binning studies, Nbs from both Sets do not share overlapping epitopes.
191 As expected, NM1221 and NM1222 (both Nb-Set2) addressed similar RBD regions compared
192 to NM1230 (**Supplementary Figure 3**). NM1224 (Nb-Set4) showed an interaction distinct from
193 all other Nbs covering besides its main binding region located at the lower right side (Front
194 View, **Figure 5**) also residues in the ACE2:RBD interface (upper left corner, Front View, **Figure**
195 **5**). As negative control, we analyzed the non-inhibitory NM1223 (Nb-Set3) (**Figure 5**) which
196 did not contact any amino acid residues involved in the RBD:ACE2 interface but rather binds
197 to the opposite site (Front View, **Figure 5**). Comparing the data from epitope binning with the
198 HDX-MS results provides structural insights into the mechanism by which non-competing pairs
199 of Nbs can simultaneously bind the RBD. Interestingly, the combination of NM1228 (Nb-Set1)
200 with NM1230 (Nb-Set2) shows a nearly complete coverage of the ACE2 interface (**Figure 5**)
201 whereas the observed inhibitory effect of NM1226 might be due to steric hindrance. In
202 conclusion, we suppose that the combination of Nb-Set1 with Nb-Set2 acts synergistically on
203 the inhibition of the interaction between RBD and ACE2.

204

205 *RBD Nbs can potently neutralize the SARS-CoV-2 virus*

206 After identification of Nbs which inhibit the RBD:ACE2 interaction biochemically, we employed
207 a cell-based viral infection assay to test for their neutralization potency. Thus, human Caco-2
208 cells were co-incubated with the icSARS-CoV-2-mNG strain and serial dilutions of the
209 inhibitory Nbs NM1224, NM1226, NM1228 and NM1230. 48 h post-infection neutralization
210 potency was determined via automated fluorescence-microscopy of fixed and nuclear-stained
211 cells. As read-out cell count and infection rate were analyzed from cell images.
212 **(Supplementary Figure 4)**. Percentage of infected cells following Nb treatment normalized to
213 a non-treated control was plotted and IC_{50} values were determined via sigmoidal inhibition
214 curve fits as the half-maximal infection. Overall, data obtained from the multiplex binding assay
215 and the viral infection assay revealed a broad consistency. Representatives of Nb-Set1,
216 NM1226 and NM1228, showed the highest neutralization potency with IC_{50} values of ~15 nM
217 and ~7 nM followed by NM1230 (~37 nM) and NM1224 (~256 nM). As expected, NM1223 (Nb-
218 Set3) was not found to reduce viral infectivity.

219 Considering that Nbs targeting diverse epitopes within the RBD:ACE2 interface are beneficial
220 to pronouncedly reduce viral infectivity and prevent mutational escape, we next combined the
221 most potent inhibitory and neutralizing candidates derived from Nb-Set1 (NM1226, NM1228)
222 and Nb-Set2 (NM1230) and tested them in the multiplex binding assay and for viral
223 neutralization. In the multiplex binding assay the combination of NM1226 and NM1230 showed
224 an increased effect in competing with ACE2 binding to RBD illustrated by a IC_{50} of 0.42 nM
225 which is 2- or 5-fold lower compared to treatment with individual NM1226 or NM1230,
226 respectively **(Figure 7 A)**. Notably, the IC_{50} measured for the combination of NM1228 and
227 NM1230 did not exceed the IC_{50} identified for NM1228 alone indicating that NM1228 by its own
228 has a very high inhibiting effect **(Figure 7 A)**. When we tested both combinations in the viral
229 infection assay, we observed significantly improved effects for both of them illustrated by an
230 IC_{50} of ~4 nM for the combination NM1226 and NM1230 and ~3.5 nM for NM1228 and NM1230
231 **(Figure 7 B, Supplementary Figure 5)**. From these findings we conclude, that a combinatorial
232 treatment with two Nbs targeting different epitopes within the RBD:ACE2 interaction site is
233 highly beneficial for viral neutralization.

234

235 *The NeurobodyPlex - High-throughput detection of neutralizing antibodies in serum samples*
236 *of patients after SARS-CoV-2 infection*

237 Recently, several serological assays analyzing the immune response in infected and
238 recovered SARS-CoV-2 patients have been published [17, 18, 20-22]. These assays provide
239 data on the presence and distribution of antibody subtypes against the SARS-CoV-2 within
240 serum samples. However, while those testing systems detect the overall antibody response
241 against distinct antigens of SARS-CoV-2, they do not provide the answer to the most relevant
242 question whether the tested individuals carry neutralizing antibodies which prevent reinfection.
243 In this context, multiple studies have convincingly shown that neutralizing antibodies preferable
244 bind to the RBD domain and sterically inhibit viral entry via ACE2 [1, 3]. This let us assume
245 that our RBD Nbs covering large parts of the RBD:ACE2 interface might be suitable to monitor
246 the emergence and presence of neutralizing antibodies in patients. To test this hypothesis, we
247 set up a high-throughput competitive binding assay, termed NeurobodyPlex, by combining our
248 most potent neutralizing Nb combinations with a recently developed, automatable multiplex
249 immunoassay (**Figure 8 A**) [18]. We incubated our previously generated color-coded beads
250 comprising RBD, S1 domain or homotrimeric Spike with serum samples from patients or non-
251 infected individuals in addition to dilution series of the combinations NM1226/ NM1230 or
252 NM1228/ NM1230 followed by the detection of patient-derived IgGs bound to the respective
253 antigens. Depending on the Nb concentration, neutralizing antibodies targeting the RBD:ACE2
254 interaction site within the serum samples are displaced resulting in a reduction of the
255 detectable signal (**Figure 8 A**).

256 By analyzing RBD specific IgGs from serum samples, we detected a distinct signal reduction
257 in the presence of increasing Nb concentrations for all tested samples (**Figure 8 B**,
258 **Supplementary Figure 6 A**) indicating that all patients comprise a substantial fraction of RBD-
259 reactive IgGs targeting the RBD:ACE2 interface. Notably, we observed no changes when
260 analyzing competitive binding for IgGs addressing the homotrimeric Spike protein, which

261 suggests the presence of multiple IgGs targeting epitopes beyond the RBD:ACE2 interaction
262 site (**Figure 8 B, Supplementary Figure 6 A**).

263 To further demonstrate that our approach is able to determine the presence of IgGs targeting
264 the RBD:ACE2 interaction site in detailed resolution, we highlighted the effect of competing
265 Nbs on two selected serum samples. For sample #289 we observed a clear displacement of
266 IgGs when we measured antibody binding to RBD and S1 domain upon addition of competing
267 Nbs, while for sample #265 only a slight reduction of the IgG signal on S1 domain was
268 detectable (**Figure 8 C, Supplementary Figure 6 B**). Additionally, we compared our
269 NeurobodyPlex approach using RBD-specific Nbs with conventional antibodies by applying
270 the neutralizing mouse antibody MM43 [19] in a similar setting. Here we detected substantial
271 cross-reactive signals from the labeled anti-human-IgG in all five serum samples
272 (**Supplementary Figure 6 C**). From those findings we conclude, that mouse antibodies are
273 not suitable, as they bear the risk to be falsely detected. In summary, our data revealed that
274 the NeurobodyPlex provides a suitable screening system to monitor the presence of RBD-
275 targeting antibodies in patient samples which can be reliably considered to mediate a
276 neutralizing and protective immune response.

277

278 Finally, we validated our NeurobodyPlex by analyzing a cohort of 18 serum samples of
279 convalescent SARS-CoV-2 patients and four control samples from healthy donors using one
280 consistent Nb concentration (1.26 μ M). Within the tested serum cohort all donors infected with
281 SARS-CoV-2 showed the presence of neutralizing antibodies, most clearly visible when using
282 RBD as antigen (**Figure 9 A, Supplementary Figure 7**). For direct comparison with the a cell-
283 based viral infection assay as the gold standard for detecting neutralizing serum antibodies
284 [23], we tested the same sample cohort in dilution series using the previously described
285 icSARS-CoV-2-mNG strain in Caco-2 cells (**Figure 9 B**). The viral infection assay revealed the
286 presence of neutralizing antibodies in the same sample set derived from convalescent SARS-
287 CoV-2 patients, whereas none of the samples from healthy donors showed any effect.
288 Observable differences between the patient samples can be explained by different antibody

289 titers, which were not investigated further. In summary, our findings showed that both
290 screening assays provide consistent information and demonstrate the suitability of our
291 NeutrobodyPlex using RBD as the most relevant antigen to reliably monitor the presence of
292 neutralizing antibodies in patients.

293

294 **Discussion**

295 Indisputably, there is a strong need for diagnostic tools and therapeutics against SARS-CoV-
296 2 infection. As demonstrated for neutralizing antibodies selected from convalescent COVID-
297 19 patients, biologically-derived binding molecules can effectively address the large interaction
298 site of the RBD domain of SARS-CoV-2 and the ACE2 receptor exposed on human lung
299 epithelium [3, 24, 25]. A promising alternative to conventional antibodies are Nbs derived either
300 from naïve/ synthetic libraries or immunized camelids [26]. By employing suitable screening
301 strategies, Nbs addressing predefined domains within larger antigens can be selected. Since
302 the description of the first Nb shown to bind the RBD of homotrimeric Spike protein of SARS-
303 CoV-2 [6], multiple well working Nbs targeting this particular viral domain have been identified
304 [7, 8, 10, 11]. In this study we identified 11 novel RBD-specific Nbs derived from an immunized
305 animal (*Vicugna pacos*). According to their sequences these Nbs can be clustered in 8 unique
306 families representing different germ lines which indicates a prominent immune response
307 towards the fully glycosylated antigen. All identified monovalent Nbs except NM1225 showed
308 affinities in the low nanomolar range. Thus, these Nbs do not require reformatting into bivalent
309 formats e.g. by fusing to a Fc domain or by combining multiple binding sites as previously
310 shown for other RBD targeting Nbs [6, 9, 10, 12-14].

311 For functional analysis we employed a recently developed *in vitro* multiplex binding assay [18]
312 to monitor the replacement of ACE2 as the natural ligand from binding to RBD, S1 domain or
313 homotrimeric Spike upon addition of RBD-specific Nbs. With this assay we were able to identify
314 eight inhibiting Nbs targeting those Spike-derived antigens. Interestingly, IC₅₀ values obtained
315 for inhibitory Nbs on RBD and homotrimeric Spike show a higher correlation compared to IC₅₀
316 values obtained for the S1 domain. Based on a detailed epitope mapping, we grouped our Nbs
317 in five different Nb-Sets. Three of those Nb-Sets are comprising inhibitory Nbs, which were
318 shown to target different epitopes within the RBD:ACE2 interaction site. We confirmed the
319 neutralizing potency of those Nbs in a cell-based viral infection assay using fully intact SARS-
320 CoV-2. By this we noted that the measurable viral neutralization effect of the individual Nbs
321 strongly correlates to the data obtained from the biochemical screen, which demonstrates that

322 the multiplex binding assay as presented is highly relevant and suitable to identify virus
323 neutralizing binders. Based on these findings we modified our previously described multiplex
324 immunoassay (MULTICOV-AB, [18]) and developed a novel diagnostic test called
325 NeutrobodyPlex to monitor the presence and the emergence of neutralizing antibodies in
326 serum samples of SARS-CoV-2 infected individuals. Using combinations of high affinity Nbs
327 covering the RBD:ACE2 interface we were able to directly and specifically displace IgGs
328 present in serum samples from these particular RBD epitopes. According to previous studies
329 human IgGs addressing those epitopes were classified as neutralizing antibodies [1, 24, 25].
330 In our NeutrobodyPlex we further demonstrated that such neutralizing antibodies can be
331 detected best using the RBD. Larger Spike-derived antigens especially the full length
332 homotrimeric Spike, which is bound by a multitude of different IgGs, could be useful to
333 determine the fraction of neutralizing antibodies in a patient sample. Finally, we validated the
334 suitability of our approach by testing serum samples from 18 patients and four healthy donors
335 in comparison to the classical cell-based viral infection assay. The observed strong
336 accordance between both assays confirmed the ability of the NeutrobodyPlex to precisely
337 monitor the presence of neutralizing antibodies within patient samples.

338 To our knowledge, the NeutrobodyPlex employing Nbs blocking the RBD:ACE2 interaction site
339 shows for the first time an antigen-resolved analysis of the presence of human IgGs in
340 convalescent individuals suffering from SARS-CoV-2 infection. Compared to other neutralizing
341 serum antibody detection tests, this assay enables the analysis on an automatable high-
342 throughput basis and is performed with non-living and non-infectious viral material thus
343 reducing costs and safety conditions [23, 27]. Furthermore, the NeutrobodyPlex is highly
344 sensitive as low serum dilutions (tested dilution: 1:400) are sufficient for analysis which
345 significantly reduces patient material compared to standard assays. Considering our findings,
346 it is highly conceivable that the NeutrobodyPlex will open unique possibilities for a detailed
347 classification of the individual immune status with regard to the development of protective
348 antibodies and to monitor the efficiency of strongly needed vaccination campaigns.

349

350 **Materials and Methods**

351 **Expression constructs** For bacterial expression of Nbs, sequences were cloned into the
352 pHEN6 vector [28], thereby adding a C-terminal 6xHis-tag for IMAC purification as described
353 previously [29, 30]. The pCAGGS plasmids encoding the stabilized homotrimeric Spike protein
354 and the receptor binding domain (RBD) of SARS-CoV-2 were kindly provided by F. Krammer
355 [17]. The cDNA encoding the S1 domain (aa 1 - 681) of the SARS-CoV-2 Spike protein was
356 obtained by PCR amplification using the forward primer S1_CoV2-for 5' - CTT CTG GCG TGT
357 GAC CGG - 3' and reverse primer S1_CoV2-rev 5' - GTT GCG GCC GCT TAG TGG TGG
358 TGG TGG TGG TGG GGG CTG TTT GTC TGT GTC TG - 3' and the full length SARS-CoV-
359 2 Spike cDNA as template and cloned into the XbaI/ NotI-digested backbone of the pCAGGS
360 vector, thereby adding a C-terminal His₆-Tag. All expression constructs were verified by
361 sequence analysis.

362

363 **V_HH libraries** Alpaca immunizations with purified RBD and V_HH-library construction were
364 carried out as described previously [31]. Animal immunization has been approved by the
365 government of Upper Bavaria (Permit number: 55.2-1-54-2532.0-80-14). In brief, nine weeks
366 after immunization of an animal (*Vicugna pacos*) with either C-terminal histidine-tagged RBD
367 (RBD-His₆), ~100 ml blood were collected and lymphocytes were isolated by Ficoll gradient
368 centrifugation using the Lymphocyte Separation Medium (PAA Laboratories GmbH). Total
369 RNA was extracted using TRIzol (Life Technologies) and mRNA was reverse transcribed to
370 cDNA using a First-Strand cDNA Synthesis Kit (GE Healthcare). The V_HH repertoire was
371 isolated in 3 subsequent PCR reactions using following primer combinations (1) CALL001 (5'-
372 GTC CTG GCT GCT CTT CTA CA A GG-3') and CALL002 (5'-GGT ACG TGC TGT TGA ACT
373 GTT CC-3') (2) forward primer set FR1-1, FR1-2, FR1-3, FR1-4 (5'-CAT GGC NSA NGT GCA
374 GCT GGT GGA NTC NGG NGG-3', 5'-CAT GGC NSA NGT GCA GCT GCA GGA NTC NGG
375 NGG-3', 5'-CAT GGC NSA NGT GCA GCT GGT GGA NAG YGG NGG-3', 5'-CAT GGC NSA
376 NGT GCA GCT GCA GGA NAG YGG NGG-3') and reverse primer CALL002 and (3) forward
377 primer FR1-ext1 and FR1-ext2 (5'-GTA GGC CCA GCC GGC CAT GGC NSA NGT GCA GCT

378 GGT GG-3', 5'-GTA GGC CCA GCC GGC CAT GGC NSA NGT GCA GCT GCA GGA-3' A-)
379 and reverse primer set FR4-1, FR4-2, FR4-3, FR4-4, FR4-5 and FR4-6 (5'-GAT GCG GCC
380 GCN GAN GAN ACG GTG ACC NGN RYN CC-3'. 5'-GAT GCG GCC GCN GAN GAN ACG
381 GTG ACC NGN GAN CC-3'. 5'-GAT GCG GCC GCN GAN GAN ACG GTG ACC NGR CTN
382 CC-3'. 5'-GAT GCG GCC GCR CTN GAN ACG GTG ACC NGN RYN CC-3'. 5'-GAT GCG
383 GCC GCR CTN GAN ACG GTG ACC NGN GAN CC-3'. 5'-GAT GCG GCC GCR CTN GAN
384 ACG GTG ACC NGR CTN CC-3') introducing SfiI and NotI restriction sites. The V_HH library
385 was subcloned into the SfiI/ NotI sites of the pHEN4 phagemid vector [28]

386

387 **V_HH Screening** For the selection of RBD-specific V_HHs two consecutive phage enrichment
388 rounds were performed. Therefore, TG1 cells containing the 'immune'-library in pHen4 were
389 infected with the M13K07 helper phage, hence the V_HH domains were presented superficial
390 on phages. For each round 1 x 10¹¹ phages of the 'immune'-library were applied on RBD either
391 directly coated on immunotubes (10 µg/ml) or biotinylated RBD (5 µg/ml) immobilized on 96-
392 well plates pre-coated with Streptavidin. In each selection round extensive blocking of antigen
393 and phages was performed by using 5% milk or BSA in PBS-T and with increasing panning
394 round PBS-T washing stringency was intensified. Bound phages were eluted in 100 mM tri-
395 ethylamind, TEA (pH 10.0), followed by immediate neutralization with 1 M Tris/HCl (pH 7.4).
396 For phage preparation for following rounds, exponentially growing TG1 cells were infected and
397 spread on selection plates. Antigen-specific enrichment for each round was monitored by
398 comparing colony number of antigen vs. no antigen selection. Following panning 492 individual
399 clones of the second selection round were screened by standard Phage-ELISA procedures
400 using a horseradish peroxidase-labeled anti-M13 monoclonal antibody (GE-Healthcare).

401

402 **Protein expression and purification** RBD-specific Nbs were expressed and purified as
403 previously published [29, 30]. For the expression of SARS-CoV-2 proteins (RBD, stabilized
404 homotrimeric Spike and S1 domain) Expi293 cells were applied in agreement to the protocol
405 of Stadlbauer *et al.* [32]. For quality control all purified proteins were analyzed via SDS-PAGE

406 according to standard procedures. Therefore, protein samples were denaturated (5 min, 95°C)
407 in 2x SDS-sample buffer containing 60 mM Tris/HCl, pH 6.8; 2% (w/v) SDS; 5% (v/v)
408 2-mercaptoethanol, 10% (v/v) glycerol, 0.02% bromphenole blue. All proteins were visualized
409 by InstantBlue Coomassie (Expedeon) staining. For immunoblotting proteins were transferred
410 on nitrocellulose membrane (Bio-Rad Laboratories) and detection was performed using anti-
411 His primary antibody (Penta-His Antibody, #34660, Qiagen) followed by donkey-anti-mouse
412 secondary antibody labeled with AlexaFluor647 (Invitrogen) using a Typhoon Trio scanner
413 (GE-Healthcare, Freiburg, Germany; excitation 633 nm, emission filter settings 670 nm BP 30).
414

415 **Biophysical biolayer interferometry (BLI)** For analyzing the binding affinity of purified Nbs
416 towards RBD biolayer interferometry (BLItz, ForteBio) was performed. Therefore, biotinylated
417 RBD was immobilized on single-use high-precision streptavidin biosensors (SAX) according to
418 manufacturer's protocols. Depending on the affinity of the RBD-Nb interaction, an appropriate
419 concentration range (15.6 nM-2 µM) of Nbs was used. In total for each run four different Nb
420 concentrations were measured as well as a reference run using PBS instead of Nb in the
421 association step. As negative control the GFP-Nb (500 nM) was applied in the binding studies.
422 By this means, global fits were obtained using the BLItzPro software and the global dissociation
423 constant (K_D) was calculated. For the epitope competition analysis biotinylated RBD was
424 immobilized on streptavidin sensor in the same fashion as for the affinity measurements. By
425 two consecutive application steps each with association and short dissociation of two different
426 Nbs (500nM) competition binding was performed.

427
428 **Bead-based multiplex binding/ competition assay** Purified RBD, S1 domain and
429 homotrimeric Spike of SARS-CoV-2 were covalently immobilized on spectrally distinct
430 populations of carboxylated paramagnetic beads (MagPlex Microspheres, Luminex
431 Corporation, Austin, TX) using 1-ethyl-3-(3-dimethylaminopropyl)carbodiimide (EDC)/ sulfo-N-
432 hydroxysuccinimide (sNHS) chemistry. For immobilization, a magnetic particle processor
433 (KingFisher 96, Thermo Scientific, Schwerte, Germany) was used. Bead stocks were vortexed

434 thoroughly and sonicated for 15 seconds. Subsequently, 83 μL of 0.065% (v/v) Triton X-100
435 and 1 mL of bead stock containing 12.5×10^7 beads of one single bead population were
436 pipetted into each well. The beads were then washed twice with 500 μL of activation buffer
437 (100 mM Na_2HPO_4 , pH 6.2, 0.005% (v/v) Triton X-100) and activated for 20 min in 300 μL of
438 activation mix containing 5 mg/mL EDC and 5 mg/mL sNHS in activation buffer. Following
439 activation, the beads were washed twice with 500 μL of coupling buffer (500 mM MES, pH 5.0,
440 0.005% (v/v) Triton X-100) and the proteins were added to the activated beads and incubated
441 for 2 h at 21 °C to immobilize the antigens on the surface. Protein-coupled beads were washed
442 twice with 800 μL of wash buffer (1x PBS, 0.005 % (v/v) Triton X-100) and were finally
443 resuspended in 1,000 μL of storage buffer (1x PBS, 1 % (w/v) BSA, 0.05% (v/v) ProClin). The
444 beads were stored at 4°C until further use. For bead-based multiplex assays, individual bead
445 populations were combined into a bead mix.

446 For the bead-based ACE2 competition binding assay, Nbs were incubated with the bead-mix
447 containing beads coupled with SARS-CoV-2 homotrimeric Spike, RBD and S1 proteins in the
448 presence of biotinylated ACE2 (Sino Biological) competing for the binding of SARS-CoV-2
449 spike-derived antigens. Single Nbs or Nb combinations were pre-diluted to a concentration of
450 6.3 $\mu\text{mol/L}$ per Nb in assay buffer. Afterwards, a 4-fold dilution series was made over eight
451 steps in assay buffer containing 160 ng/mL biotinylated ACE2. Subsequently, 25 μL of every
452 dilution was transferred to 25 μL bead-mix in a 96-well half-area plate. The plate was incubated
453 for 2 h at 21 °C, shaking at 750 rpm. Afterwards, the beads were washed using a microplate
454 washer (Biotek 405TS, Biotek Instruments GmbH) to remove unbound ACE2 or Nbs. The
455 beads were then incubated with R-phycoerythrin-labeled streptavidin to detect biotinylated
456 ACE2 that bound to the immobilized antigen for 45 minutes at 21 °C shaking at 750 rpm.
457 Afterwards, the beads were washed again to remove unbound PE-labeled streptavidin.
458 Measurements were performed with a FLEXMAP 3D instrument using the xPONENT Software
459 version 4.3 (settings: sample size: 80 μL , 50 events, Gate: 7,500 – 15,000, Reporter Gain:
460 Standard PMT).

461

462 **NeutrobodyPlex: Bead-based multiplex neutralizing antibody detection assay** Based on
463 the recently described automatable multiplex immunoassay by Becker *et al.* [18], the
464 NeutrobodyPlex was developed and similar assay conditions were applied. For the detection
465 of neutralizing serum antibodies the bead-mix containing beads coupled with purified RBD, S1
466 domain or homotrimeric Spike of SARS-CoV-2 was incubated with Nb combinations
467 (concentrations ranging from 1.26 μM to 0.08 nM for each Nb) and serum samples of
468 convalescent SARS-CoV-2 patients and healthy donors at a 1:400 dilution. As positive control
469 and maximal signal detection per sample, serum only was included and as negative control for
470 Nb binding a SARS-CoV-2-unspecific GFP nanobody (1.26 μM) was used. For comparison of
471 Nb performance the inhibiting mouse antibody (40591-MM43) was applied in concentrations
472 of 0.17 μM to 0.08 nM. Bound serum IgG were detected via anti-human-IgG-PE as previously
473 described [18].

474

475 **Hydrogen-Deuterium Exchange**

476 *RBD Deuteration Kinetics and Epitope Elucidation*

477 RBD (5 μL , 73 μM) was either incubated with PBS or RBD-specific Nbs (2.5 μL , 2.5 mg/mL in
478 PBS) at 25 °C for 10 min. Deuterium exchange of the pre-incubated nanobody-antigen
479 complex was initiated by dilution with 67.5 μL PBS (150 mM NaCl, pH 7.4) prepared with D_2O
480 and incubation for 5 and 50 minutes respectively at 25 °C. To ensure a minimum of 90% of
481 complex formation, the molar ratio of antigen to Nbs was calculated according to Kochert *et al.*
482 [33] using the affinity constants of 1.37 nM (NM1228), 3.66 nM (NM1226), 3.82 nM (NM1223),
483 8.23 nM (NM1230) and 8.34 nM (NM1224) determined by BLI analysis. The final D_2O
484 concentration was 90%. After 5 and 50 min at 25 °C, aliquots of 15 μL were taken and
485 quenched by adding 15 μL ice-cold quenching solution (0.2 M TCEP with 1.5% formic acid and
486 4 M guanidine HCl in 100 mM ammonium formate solution pH 2.2) resulting in a final pH of
487 2.5. Quenched samples were immediately snap frozen. The immobilized pepsin was prepared
488 by adding 60 μL of 50% slurry (in ammonium formate solution pH 2.5) to a tube and dried by
489 centrifugation at 1000 x g for 3 min at 0 °C and discarding the supernatant. Before injection,

490 aliquots were thawed and added to the dried pepsin beads. Proteolysis was performed for 2
491 min in a water ice bath followed by filtration using a 22 μm filter and centrifugation at 1000 x g
492 for 30 s at 0 °C. Samples were immediately injected to a LC-MS system. Undeuterated control
493 samples were prepared under the same conditions using H₂O instead of D₂O. The same
494 protocol was applied for the Nbs without addition of RBD as well to create a list of peptic
495 peptides. The HDX experiments of the RBD-Nb-complex were performed in triplicates. The
496 back-exchange of the method as determined using a standard peptide mixture of 14 synthetic
497 peptides was 24%.

498

499 *Chromatography and Mass Spectrometry*

500 HDX samples were analyzed on a LC-MS system comprised of RSLC pumps (UltiMate 3000
501 RSLCnano, Thermo Fisher Scientific, Dreieich, Germany), a chilling device for
502 chromatography (Mécour Temperature Control, Groveland, MA, USA) and a mass
503 spectrometer Q Exactive (Thermo Fisher Scientific, Dreieich, Germany). The chilling device
504 contained the LC column (ACQUITY BEH C18, 1.7 μm , 300 Å, 1 mm x 50 mm (Waters GmbH,
505 Eschborn, Germany)), a cooling loop for HPLC solvents, a sample loop, and the injection valve
506 and kept them at 0 °C. Samples were analyzed using a two-step 20 min linear gradient with a
507 flow rate of 50 $\mu\text{l}/\text{min}$. Solvent A was 0.1% (v/v) formic acid and solvent B was 80% acetonitrile
508 (v/v) with 0.1% formic acid (v/v). After 3 min desalting at 10% B, a 9 min linear gradient from
509 10 to 25% B was applied followed by an 8 min linear gradient from 25 to 68.8%. Experiments
510 were performed using a Q Exactive (Thermo Fisher Scientific, Dreieich, Germany) with 70,000
511 resolutions instrument configurations as follows: sheath gas flow rate of 25; aux gas flow rate
512 of 5; S-lens RF level of 50, spray voltage of 3.5 kV and a capillary temperature of 300 °C.

513

514 *HDX Data Analysis*

515 A peptic peptide list containing peptide sequence, retention time and charge state was
516 generated in a preliminary LC-MS/MS experiment. The peptides were identified by exact mass
517 and their fragment ion spectrum using protein database searches by Proteome Discoverer

518 v2.1.0.81 (Thermo Fisher Scientific, Dreieich, Germany) and implemented SEQUEST HT
519 search engine. The protein database contained the RBD and the pepsin sequences. Precursor
520 and fragments mass tolerance were set to 6 ppm and 0.05 Da, respectively. No enzyme
521 selectivity was applied, however identified peptides were manually evaluated to exclude
522 peptides originated through cleavage after arginine, histidine, lysine, proline and the residue
523 after proline [34]. FDR was estimated using q-values calculated by Percolator and only
524 peptides with high-confidence identification (q-value \leq 0.01) were included to the list. Peptides
525 with overlapping mass, retention time and charge in Nb and antigen digest, were manually
526 removed. The deuterated samples were recorded in MS mode only and the generated peptide
527 list was imported into HDEaminer v2.5.0 (Sierra Analytics, Modesto, CA, USA). Deuterium
528 uptake was calculated using the increase of the centroid mass of the deuterated peptides.
529 HDX could be followed for 79% of the RBD amino acid sequence. The calculated percentage
530 deuterium uptake of each peptide between RBD-Nb and RBD-only were compared. Any
531 peptide with uptake reduction of 5% or greater upon Nb binding was considered as protected.

532

533 **Cell culture** Caco-2 (Human Colorectal adenocarcinoma) cells were cultured at 37°C with 5%
534 CO₂ in DMEM containing 10% FCS, with 2 mM l-glutamine, 100 µg/ml penicillin-streptomycin
535 and 1% NEAA.

536

537 **Viruses** All experiments associated with the authentic virus were conducted in Biosafety Level
538 3 laboratory. The recombinant SARS-CoV-2 expressing mNeonGreen (icSARS-CoV-2-mNG)
539 (PMID: 32289263) was obtained from the World Reference Center for Emerging Viruses and
540 Arboviruses (WRCEVA) at the UTMB (University of Texas Medical Branch). To generate
541 icSARS-CoV-2-mNG stocks, 200.000 Caco-2 cells were infected with 50 µl of virus in a 6-well
542 plate, the supernatant was harvested 48 hpi, centrifuged, and stored at -80°C. For MOI
543 determination, a titration using serial dilutions of the mNeonGreen (icSARS-CoV-2-mNG) was
544 conducted. The number of infectious virus particles per ml was calculated as the (MOI × cell
545 number) / (infection volume), where $MOI = -\ln(1 - \text{infection rate})$.

546

547 **Neutralization assay** For neutralization experiments, 1×10^4 Caco-2 cells/well were seeded in
548 96-well plates the day before infection in media containing 5% FCS. Caco-2 cells were co-
549 incubated with the SARS-CoV-2 strain icSARS-CoV-2-mNG at a MOI=1.1 and Nbs or serum
550 samples in serial dilutions in the indicated concentrations. 48 hpi cells were fixed with 2% PFA
551 and stained with Hoechst33342 (1 $\mu\text{g}/\text{mL}$ final concentration) for 10 minutes at 37°C. The
552 staining solution was removed and exchanged for PBS. For quantification of infection rates,
553 images were taken with the Cytation3 (Biotek) and Hoechst+ and mNG+ cells were
554 automatically counted by the Gen5 Software (Biotek). Data were normalized to respective
555 virus-only infection control. Inhibitory concentration 50 (IC_{50}) was calculated as the half-
556 maximal inhibitory dose using 4-parameter nonlinear regression (GraphPad Prism).

557

558 **Patient samples** A total of 23 serum samples from SARS-CoV-2 convalescent patients (#xxx)
559 and 4 healthy donors (C1-4) were analyzed in the course of this study. All samples used were
560 de-identified and pre-existing. Ethical consent was granted from the Ethics commission of the
561 University of Tuebingen under the votum 179/2020/BO2. Samples were classified as SARS-
562 CoV-2 infected, due to a self-reported positive SARS-CoV-2 RT-PCR.

563

564 **Analyses and Statistics** Graph preparation and statistical analysis was performed using the
565 GraphPad Prism Software (Version 8.3.0).

566

567

568 **Data availability**

569 The data that support the findings of this study are available from the corresponding authors
570 upon reasonable request.

571

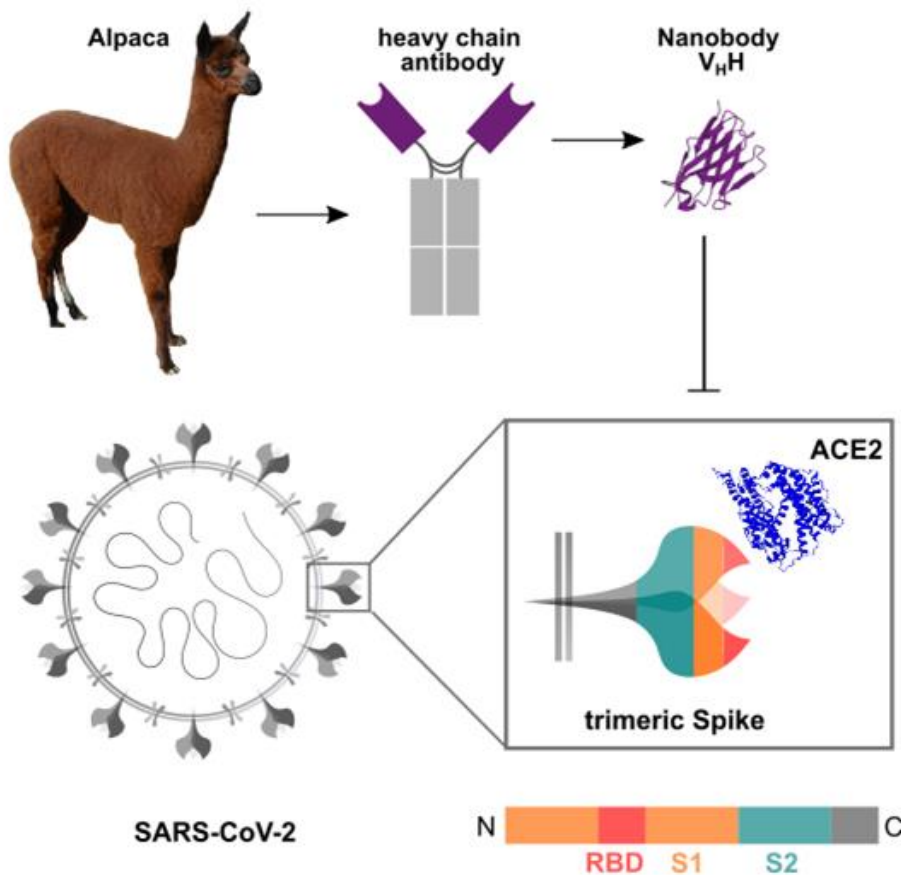
572 **Authorship Contributions**

573 N.S.M., T.W., M.B. and U.R. designed the study; P.D.K., B.T. T.W. performed Nb selection
574 and biochemical characterization; H.S., S.N., A.S. immunized the animal; J.H., D.J., M.B.,
575 performed the multiplex binding assay; M.G., A.Z. performed HDX-MS experiments; Mo.S.,
576 G.K. A.N., J.S.W. and K.S.L. organize and provide patient samples; N.R.B., M.S. performed
577 viral neutralization assays; T.W., M.B., J.H., M.G., A.Z., N.R.B., M.S. and U.R. analyzed data
578 and performed statistical analysis. T.W. and U.R. drafted the manuscript; N.S.M., U.R.
579 supervised the study. All authors critically read the manuscript.

580

581

582 **Figures:**



583

584 **Figure 1 Schematic depiction of the generation of Nbs blocking the SARS-CoV-2**

585 **RBD:ACE2 interaction site**

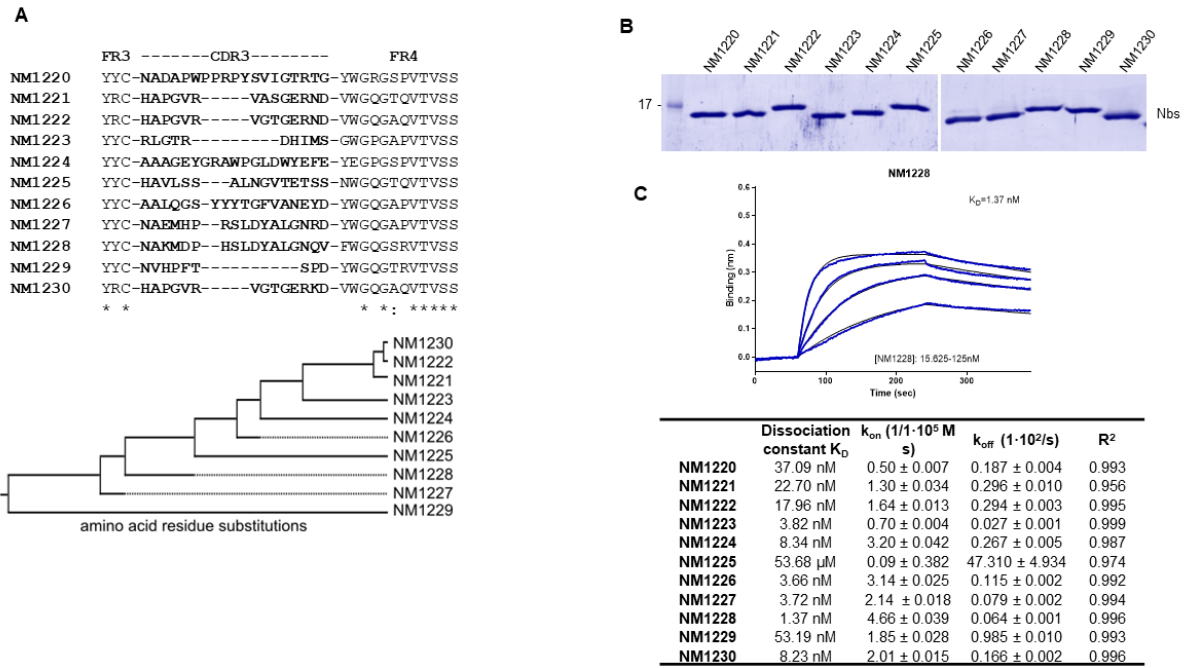
586 Nanobodies (Nbs) are genetically engineered from heavy chain only antibodies of alpacas.

587 The interaction between the SARS-CoV-2 homotrimeric Spike protein and ACE2 can be

588 blocked by RBD-specific Nbs. Protein structures adapted from PDB 3OGO (Nb) and 6CS2

589 (ACE2).

590

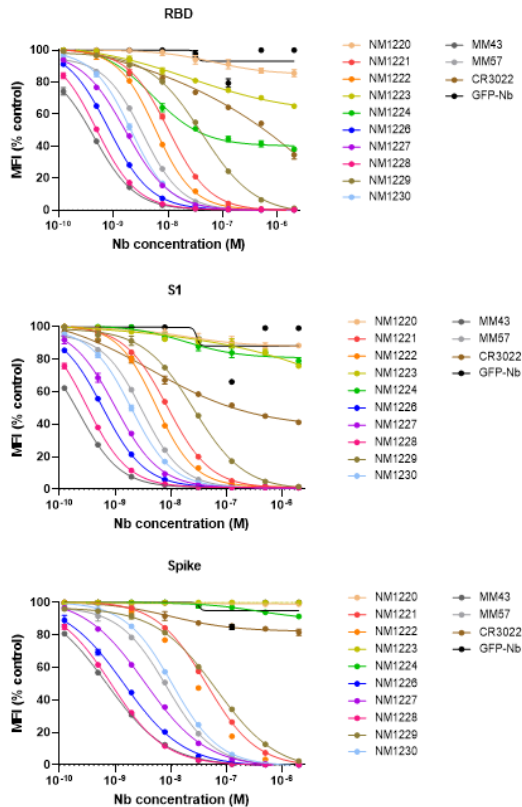


591

592 **Figure 2: Selection of nanobodies (Nbs) against RBD**

593 **(A)** Amino acid sequences of the complementarity determining region (CDR) 3 from unique
594 Nbs selected after two rounds of biopanning are listed (upper panel). Phylogenetic tree based
595 on a ClustalW alignment of the CDR3 sequences is shown (lower panel). **(B)** Recombinant
596 expression and purification of Nbs using immobilized metal affinity chromatography (IMAC)
597 and size exclusion chromatography (SEC). Coomassie staining of 2 μ g of purified Nbs is
598 shown **(C)** For biolayer interferometry (BLI)-based affinity measurements, biotinylated RBD
599 was immobilized on streptavidin biosensors. Kinetic measurements were performed by using
600 four concentrations of purified Nbs ranging from 15.6 nM - 2 μ M. As an example the sensogram
601 of NM1228 at indicated concentrations is shown (upper panel). The table summarizes affinities
602 (K_D), association (K_{on}) and dissociation constants (K_{off}) determined for individual Nbs (lower
603 panel).

604



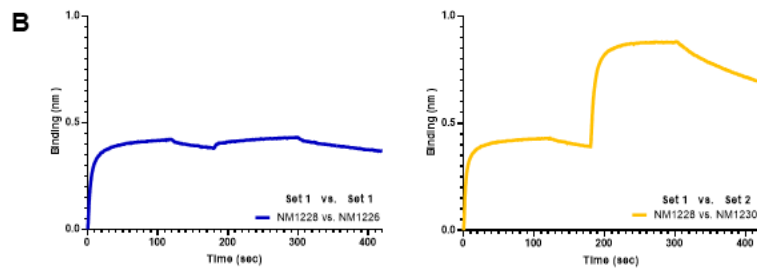
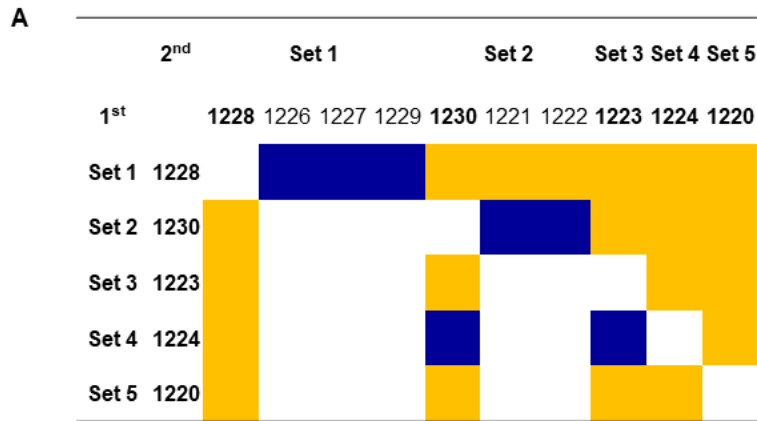
	IC ₅₀ (nM) ACE2:RBD Inhibition	IC ₅₀ (nM) ACE2:S1 Inhibition	IC ₅₀ (nM) ACE2:Spike Inhibition
NM1220	NA	NA	NA
NM1221	10.14	43.28	8.95
NM1222	5.80	27.28	5.50
NM1223	NA	NA	NA
NM1224	36.58	NA	NA
NM1226	0.82	1.44	0.63
NM1227	1.65	3.51	1.06
NM1228	0.50	0.85	0.32
NM1229	37.83	56.07	24.95
NM1230	2.12	10.57	1.96
GFP-Nb	NA	NA	NA
40591-MM43	0.38	0.71	0.20
40592-MM57	3.22	7.83	2.93
CR3022	585.27	2016.00	141.26

605

606 Figure 3: Multiplex binding assay to identify inhibitory Nbs

607 Results from bead-based multiplex ACE2 competition assay are shown for the three SARS-
 608 CoV-2 Spike-derived antigens, RBD, S1 and homotrimeric Spike. ACE2 bound to the
 609 respective antigen was detected. For each Nb, a dilution series over eight steps (2.106 μ M to
 610 0.123 nM) is shown in the presence of 80 ng/mL ACE2. MFI signals were normalized to the
 611 maximal signal per antigen as given by the ACE2-only control. IC₅₀ values were calculated
 612 from a four-parametric sigmoidal model and are displayed for each Nb and antigen. Data are
 613 presented as mean \pm stds of three technical replicates (n =3).

614

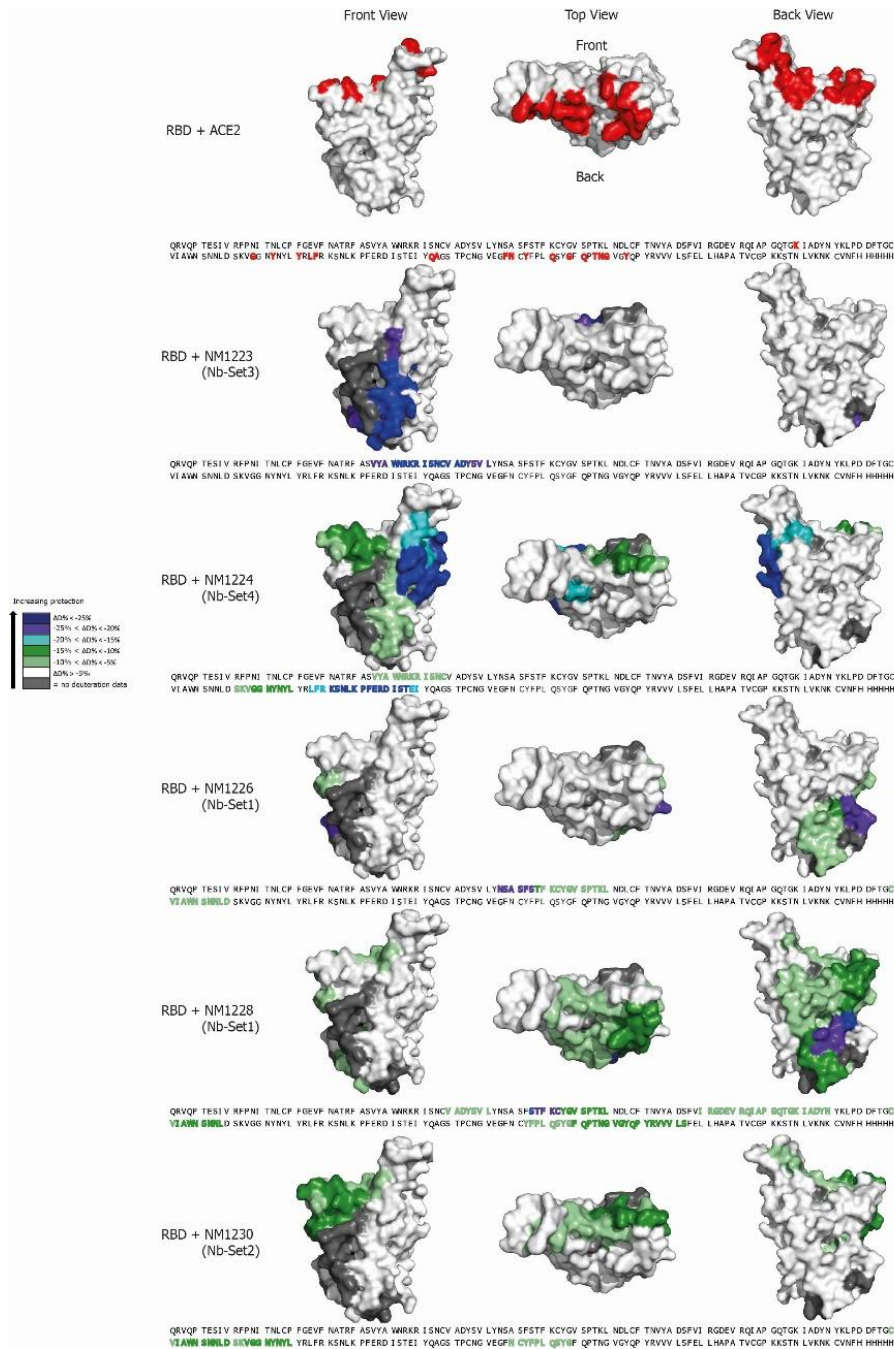


615

616 **Figure 4 Epitope binning of Nbs**

617 **(A)** Heat map illustration of competitive Nb epitope binning on RBD using biolayer
618 interferometry (BLI). Rows and columns represent the loading of the first and second Nb,
619 respectively. Blue colored squares illustrate no additional binding of the second Nb meaning
620 both Nbs belong to the same Nb-Set. Orange colored squares represent additional binding of
621 the second Nb, hence these Nbs belong to different Nb-Sets. **(B)** Representative sensograms
622 of single BLI measurements of Nbs affiliated to the same Nb-Set (NM1228/ NM1226, blue) and
623 to different Nb-Sets (NM1228/ NM1230, orange) are shown.

624

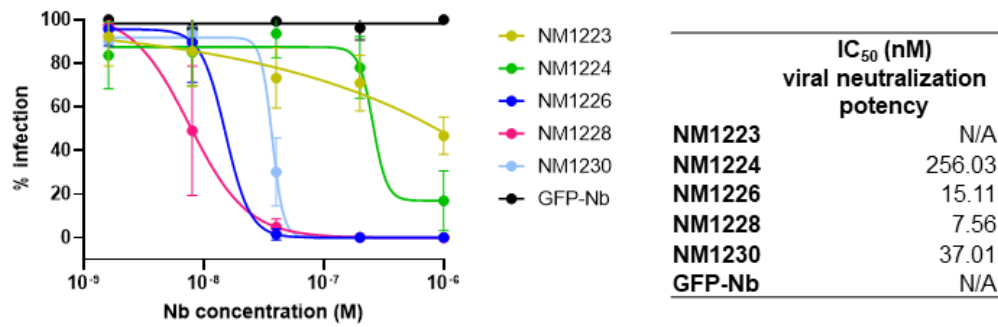


625

626 **Figure 5: Epitope mapping of Nbs by HDX mass spectrometry**

627 Surface structure model of the RBD showing the ACE2 interface and the HDX-MS epitope
 628 mapping results of NM1223, NM1224, NM1226, NM1228, NM1230. Amino acid residues of
 629 RBD (PDB 6M17 [2]) involved in the RBD:ACE2 interaction site [2, 35] are shown in red (top
 630 panel). RBD epitopes protected upon Nb binding are highlighted in different colors indicating
 631 the strength of protection. Amino acid residues which are part of the Nb epitopes are
 632 highlighted in the RBD sequence.

633

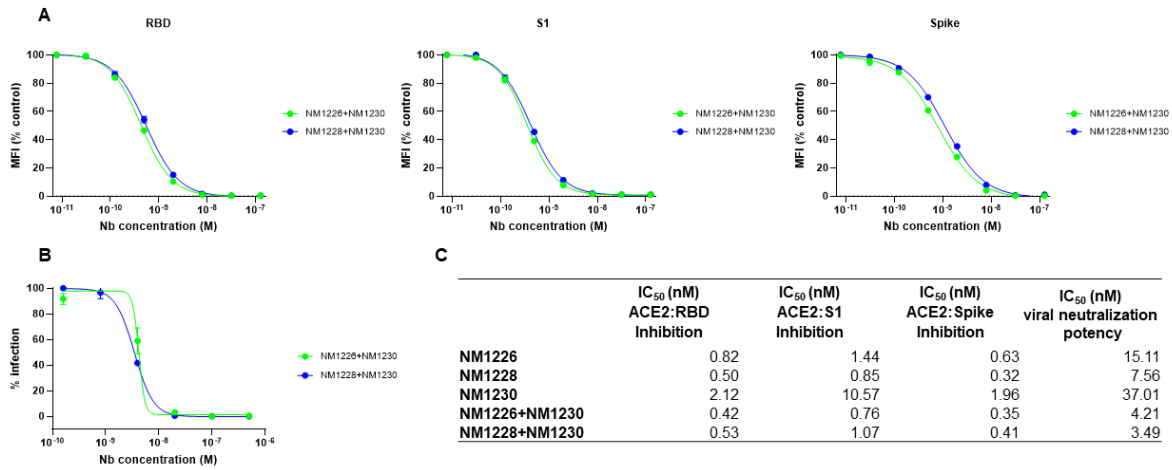


634

635 **Figure 6: Viral neutralization potency of selected Nbs**

636 (A) Inhibition of viral infectivity of the SARS-CoV-2 strain icSARS-CoV-2-mNG was analyzed
637 in Caco-2 cells using serial dilutions of NM1223, NM1224, NM1226, NM1228 and NM1230. As
638 negative control GFP-Nb was used. 48 h post-infection neutralization potency was visualized
639 via Hoechst staining and mNeonGreen expression. Intensities of mNeonGreen signal
640 normalized to virus-only infection control are illustrated as percent of infection. IC₅₀ values were
641 calculated from a four-parametric sigmoidal model and are displayed for each Nb. Data are
642 presented as mean +/- stds of three technical replicates (n =3).

643

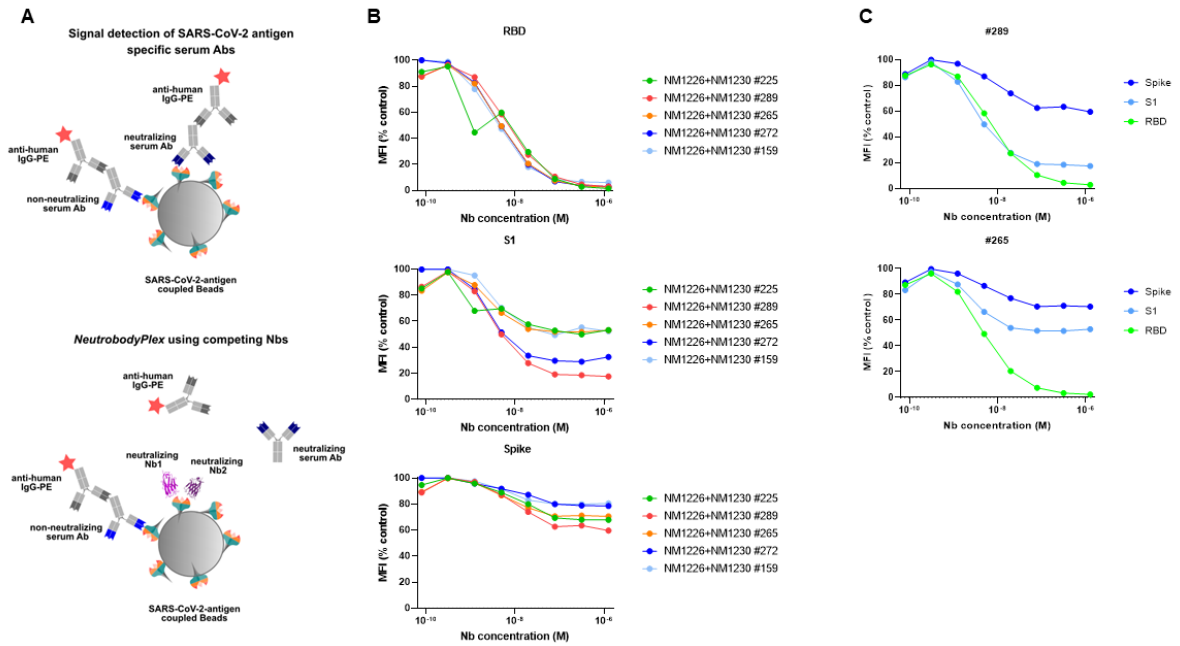


644

645 **Figure 7: Combinatorial application of RBD Nbs for inhibition of ACE2 binding and viral**
 646 **neutralization**

647 **(A)** Results from multiplex ACE2 competition assay are shown for the three Spike-derived
 648 antigens: RBD, S1 and homotrimeric Spike. Nb combinations were diluted from 126 nM to 7.69
 649 pM per Nb in the presence of 80 ng/mL ACE2 and antigen-bound ACE2 was measured. MFI
 650 signals were normalized to the maximum detectable signal per antigen given by the ACE2-
 651 only control. IC₅₀ values were calculated from a four-parametric sigmoidal model. Data are
 652 presented as mean +/- stds of three technical replicates (n =3). **(B)** Neutralization potency of
 653 Nb-Set1 (NM1226, NM1228) in combination with Nb-Set2 (NM1230) was analyzed in Caco-2
 654 cells using the SARS-CoV-2 strain icSARS-CoV-2-mNG. 48 h post-infection neutralization
 655 potency was visualized via Hoechst staining and mNeonGreen expression. Intensities of
 656 mNeonGreen signal normalized to virus-only infection control are illustrated as percent of
 657 infection. IC₅₀ values were calculated from a four-parametric sigmoidal model and are
 658 displayed for each Nb. Data are presented as mean +/- stds of two technical replicates (n = 2).
 659 **(C)** Table summarizing the IC₅₀ values obtained for the individual Nbs (as shown in **Figure 3**
 660 and **Figure 6**) and the Nb combinations.

661

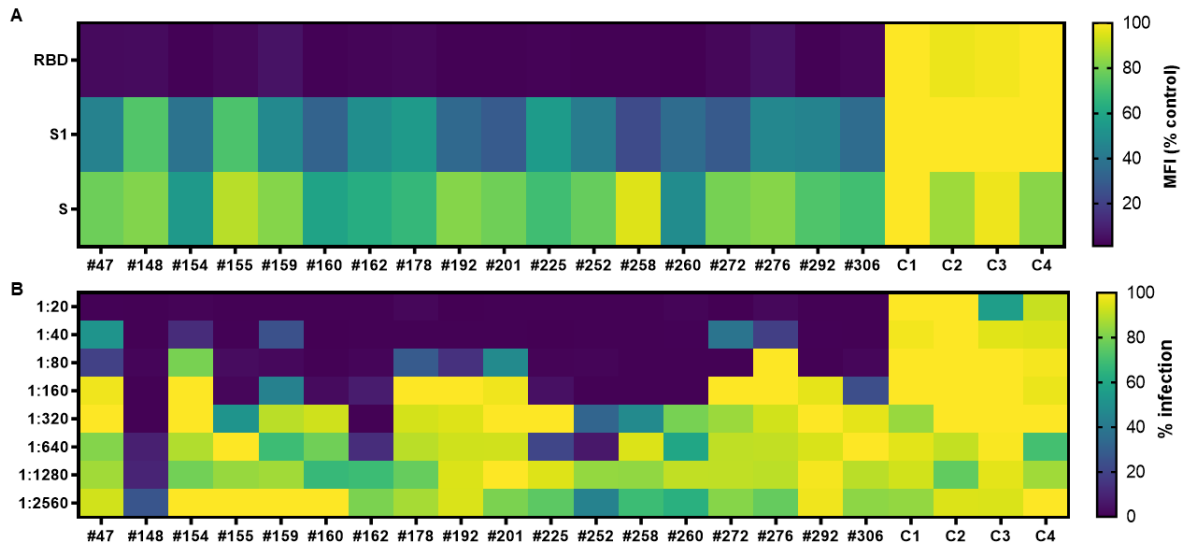


662

663 **Figure 8: The NeurobodyPlex - multiplex competitive binding assay to monitor a**
 664 **neutralizing immune response in patients**

665 **(A)** Schematic illustration of the NeurobodyPlex. The replacement of neutralizing IgGs from
 666 patient serum from binding to SARS-CoV-2 derived antigens upon addition of RBD Nbs is
 667 measured. In presence of neutralizing IgGs, the fluorescent signal from anti-human-IgG-PE, is
 668 inversely proportional to the applied Nb concentration. **(B)** For the NeurobodyPlex assay serial
 669 dilutions (1.26 μ M to 7.69 pM per Nb) of the combination NM1226/ NM1230 were incubated
 670 with five serum samples followed by detection of bound human IgGs. Shown are MFI signals
 671 obtained for all three Spike-derived antigens (RBD, S1 domain, homotrimeric Spike)
 672 normalized to serum-only control. **(C)** For two serum samples (#289, #265) differences in
 673 competition efficiency between the three Spike-derived antigens are shown.

674



675

676 **Figure 9: NeutrobodyPlex validation by testing patient samples in comparison to viral**
677 **neutralization assay**

678 (A) 18 serum samples from SARS-CoV-2 convalescent patients and four from healthy donors
679 (C1-4) were analyzed using the NeutrobodyPlex with fixed concentration of the Nb combination
680 NM1226/ NM1230 (1.26 μ M per Nb). MFI values normalized to serum only control are
681 illustrated as heat map graphic. Dark blue color coding represents loss of the detectable signal,
682 meaning a strong shift of serum antibodies into the unbound state by off-competition of Nbs.
683 Yellow color coding represents no signal differences in presence or absence of Nbs.

684 (B) The same serum samples were analyzed using the viral neutralization assay. By infecting
685 Caco-2 cells with the icSARS-CoV-2-mNG strain in presence of serial dilutions of the serum
686 samples (1:20-1:2560) the neutralization potency was determined via Hoechst staining and
687 mNeonGreen expression 48 h post-infection. Intensities of mNeonGreen signal normalized to
688 virus-only infection control are illustrated as percent of infection in a heat map graphic. Dark
689 blue color represents low mNeonGreen signal, meaning the presence of neutralizing serum
690 antibodies. Yellow color coding represents high mNeonGreen signal, indicating a lower
691 inhibition of viral infection.

692

693 **References**

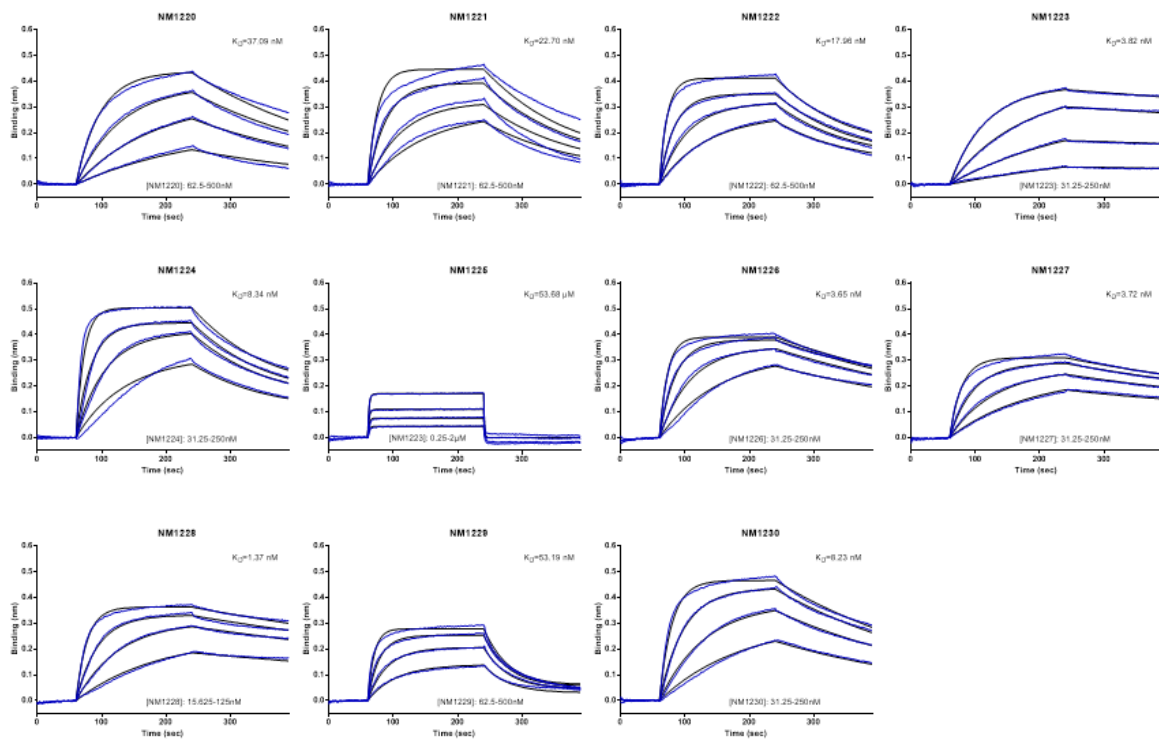
- 694 1. Rogers, T.F., et al., *Isolation of potent SARS-CoV-2 neutralizing antibodies and*
695 *protection from disease in a small animal model*. Science, 2020. **369**(6506): p. 956-
696 963.
- 697 2. Yan, R., et al., *Structural basis for the recognition of SARS-CoV-2 by full-length human*
698 *ACE2*. Science, 2020. **367**(6485): p. 1444-1448.
- 699 3. Ju, B., et al., *Human neutralizing antibodies elicited by SARS-CoV-2 infection*. Nature,
700 2020. **584**(7819): p. 115-119.
- 701 4. Tai, W., et al., *Characterization of the receptor-binding domain (RBD) of 2019 novel*
702 *coronavirus: implication for development of RBD protein as a viral attachment inhibitor*
703 *and vaccine*. Cell Mol Immunol, 2020. **17**(6): p. 613-620.
- 704 5. Muyldermans, S., *Nanobodies: natural single-domain antibodies*. Annu Rev Biochem,
705 2013. **82**: p. 775-97.
- 706 6. Wrapp, D., et al., *Structural Basis for Potent Neutralization of Betacoronaviruses by*
707 *Single-Domain Camelid Antibodies*. Cell, 2020.
- 708 7. Huo, J., et al., *Neutralizing nanobodies bind SARS-CoV-2 spike RBD and block*
709 *interaction with ACE2*. Nat Struct Mol Biol, 2020.
- 710 8. Schoof, M., et al., *An ultra-high affinity synthetic nanobody blocks SARS-CoV-2*
711 *infection by locking Spike into an inactive conformation*. bioRxiv, 2020.
- 712 9. Chi, X., et al., *Humanized Single Domain Antibodies Neutralize SARS-CoV-2 by*
713 *Targeting Spike Receptor Binding Domain*. bioRxiv, 2020: p. 2020.04.14.042010.
- 714 10. Hanke, L., et al., *An alpaca nanobody neutralizes SARS-CoV-2 by blocking receptor*
715 *interaction*. bioRxiv, 2020: p. 2020.06.02.130161.
- 716 11. Esparza, T.J., et al., *High Affinity Nanobodies Block SARS-CoV-2 Spike Receptor*
717 *Binding Domain Interaction with Human Angiotensin Converting Enzyme*. bioRxiv,
718 2020: p. 2020.07.24.219857.

- 719 12. Nieto, G.V., et al., *Fast isolation of sub-nanomolar affinity alpaca nanobody against the*
720 *Spike RBD of SARS-CoV-2 by combining bacterial display and a simple single-step*
721 *density gradient selection*. bioRxiv, 2020: p. 2020.06.09.137935.
- 722 13. Xiang, Y., et al., *Versatile, Multivalent Nanobody Cocktails for Highly Efficient SARS-*
723 *CoV-2 Neutralization*. bioRxiv, 2020: p. 2020.08.24.264333.
- 724 14. Gai, J., et al., *A potent neutralizing nanobody against SARS-CoV-2 with inhaled*
725 *delivery potential*. bioRxiv, 2020: p. 2020.08.09.242867.
- 726 15. Korber, B., et al., *Spike mutation pipeline reveals the emergence of a more*
727 *transmissible form of SARS-CoV-2*. bioRxiv, 2020: p. 2020.04.29.069054.
- 728 16. Korber, B., et al., *Tracking Changes in SARS-CoV-2 Spike: Evidence that D614G*
729 *Increases Infectivity of the COVID-19 Virus*. Cell, 2020. **182**(4): p. 812-827 e19.
- 730 17. Amanat, F., et al., *A serological assay to detect SARS-CoV-2 seroconversion in*
731 *humans*. Nat Med, 2020. **26**(7): p. 1033-1036.
- 732 18. Becker, M., et al., *Going beyond clinical routine in SARS-CoV-2 antibody testing - A*
733 *multiplex corona virus antibody test for the evaluation of cross-reactivity to endemic*
734 *coronavirus antigens*. medRxiv, 2020: p. 2020.07.17.20156000.
- 735 19. Gorshkov, K., et al., *Quantum Dot-Conjugated SARS-CoV-2 Spike Pseudo-Virions*
736 *Enable Tracking of Angiotensin Converting Enzyme 2 Binding and Endocytosis*. ACS
737 Nano, 2020.
- 738 20. Lassaunière, R., et al., *Evaluation of nine commercial SARS-CoV-2 immunoassays*.
739 medRxiv, 2020: p. 2020.04.09.20056325.
- 740 21. Robbiani, D.F., et al., *Convergent antibody responses to SARS-CoV-2 in convalescent*
741 *individuals*. Nature, 2020. **584**(7821): p. 437-442.
- 742 22. Roxhed, N., et al., *A translational multiplex serology approach to profile the prevalence*
743 *of anti-SARS-CoV-2 antibodies in home-sampled blood*. medRxiv, 2020: p.
744 2020.07.01.20143966.
- 745 23. Muruato, A.E., et al., *A high-throughput neutralizing antibody assay for COVID-19*
746 *diagnosis and vaccine evaluation*. Nat Commun, 2020. **11**(1): p. 4059.

- 747 24. Cao, Y., et al., *Potent Neutralizing Antibodies against SARS-CoV-2 Identified by High-*
748 *Throughput Single-Cell Sequencing of Convalescent Patients' B Cells*. *Cell*, 2020.
749 **182**(1): p. 73-84 e16.
- 750 25. Chi, X., et al., *A neutralizing human antibody binds to the N-terminal domain of the*
751 *Spike protein of SARS-CoV-2*. *Science*, 2020. **369**(6504): p. 650-655.
- 752 26. Rothbauer, U., *Speed up to find the right ones: rapid discovery of functional*
753 *nanobodies*. *Nat Struct Mol Biol*, 2018. **25**(3): p. 199-201.
- 754 27. Tan, C.W., et al., *A SARS-CoV-2 surrogate virus neutralization test based on antibody-*
755 *mediated blockage of ACE2-spike protein-protein interaction*. *Nat Biotechnol*, 2020.
756 **38**(9): p. 1073-1078.
- 757 28. Arbabi Ghahroudi, M., et al., *Selection and identification of single domain antibody*
758 *fragments from camel heavy-chain antibodies*. *FEBS Lett*, 1997. **414**(3): p. 521-6.
- 759 29. Kirchhofer, A., et al., *Modulation of protein properties in living cells using nanobodies*.
760 *Nat Struct Mol Biol*, 2010. **17**(1): p. 133-8.
- 761 30. Rothbauer, U., et al., *A versatile nanotrap for biochemical and functional studies with*
762 *fluorescent fusion proteins*. *Mol Cell Proteomics*, 2008. **7**(2): p. 282-9.
- 763 31. Rothbauer, U., et al., *Targeting and tracing antigens in live cells with fluorescent*
764 *nanobodies*. *Nat Methods*, 2006. **3**(11): p. 887-9.
- 765 32. Stadlbauer, D., et al., *SARS-CoV-2 Seroconversion in Humans: A Detailed Protocol for*
766 *a Serological Assay, Antigen Production, and Test Setup*. *Curr Protoc Microbiol*, 2020.
767 **57**(1): p. e100.
- 768 33. Kochert, B.A., et al., *Hydrogen-Deuterium Exchange Mass Spectrometry to Study*
769 *Protein Complexes*. *Methods Mol Biol*, 2018. **1764**: p. 153-171.
- 770 34. Hamuro, Y. and S.J. Coales, *Optimization of Feasibility Stage for Hydrogen/Deuterium*
771 *Exchange Mass Spectrometry*. *J Am Soc Mass Spectrom*, 2018. **29**(3): p. 623-629.
- 772 35. Lan, J., et al., *Structure of the SARS-CoV-2 spike receptor-binding domain bound to*
773 *the ACE2 receptor*. *Nature*, 2020. **581**(7807): p. 215-220.

775 **Supplementary Information**

776 **Supplementary Figures**

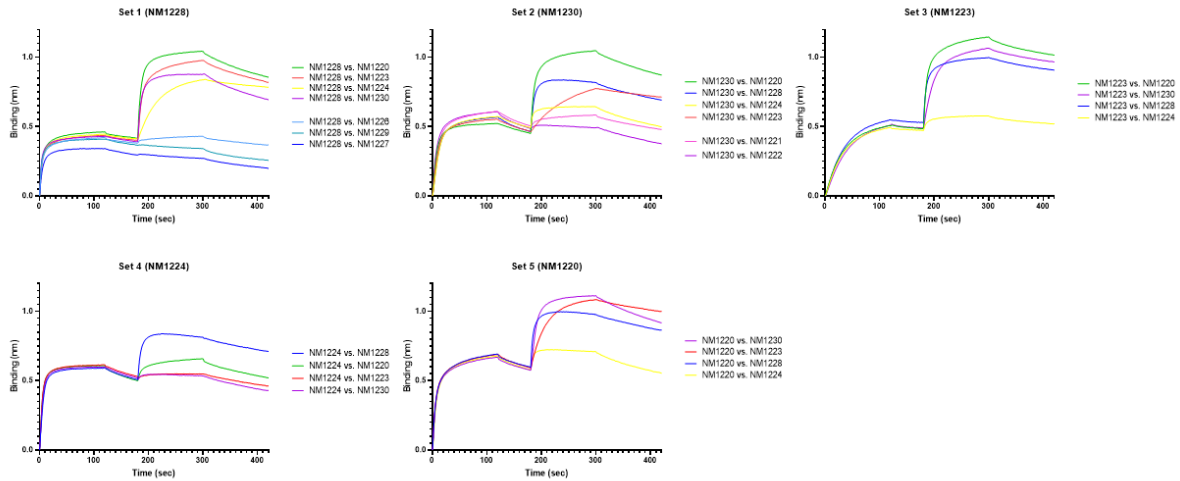


777

778 **Supplementary Figure 1: Affinities of RBD binding Nbs determined by biolayer**
779 **interferometry**

780 Sensograms of biolayer interferometry-based affinity measurements of 11 identified SARS-
781 CoV-2 RBD Nbs are shown. For analysis biotinylated RBD was immobilized on streptavidin
782 biosensors and kinetic measurements were performed by using four concentrations of purified
783 Nbs ranging from 15.6 nM - 2 μ M.

784



785

786 **Supplementary Figure 2: Epitope binning of SARS-CoV-2 RBD Nbs**

787 Sensograms of biolayer interferometry-based epitope binning of dual Nb binding are shown.

788 Biotinylated RBD was immobilized on streptavidin biosensors followed by two consecutive

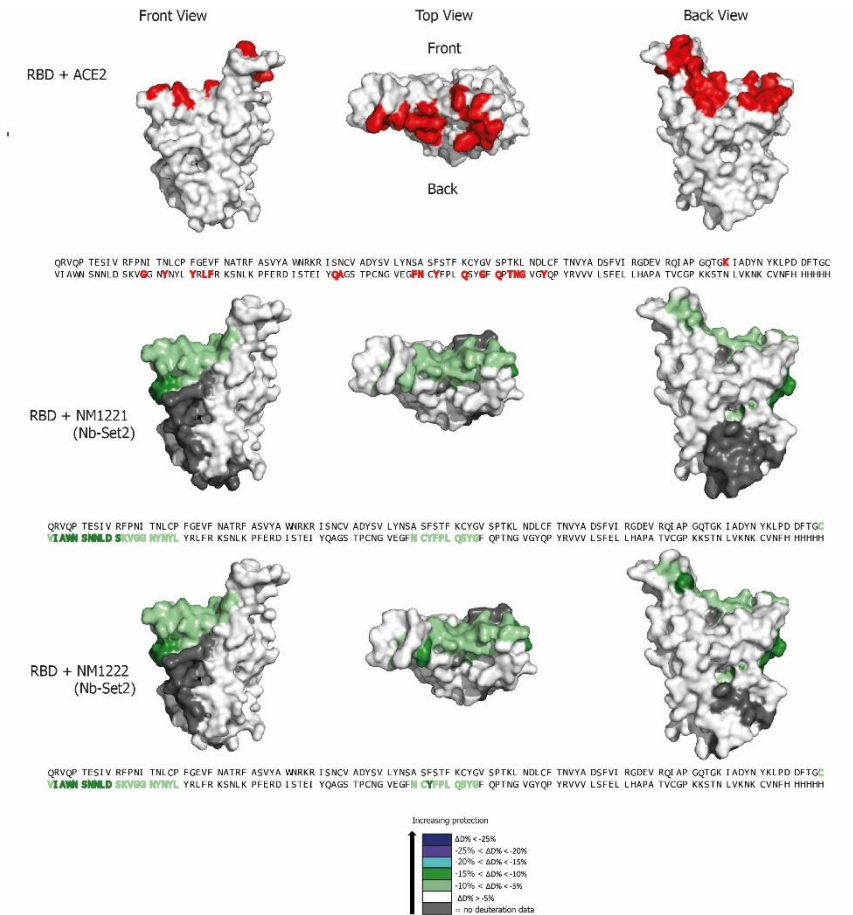
789 loading steps of different RBD Nbs. Depending on additional loading (different epitope) or non-

790 loading (similar/ overlapping epitope) of the second Nb, Nbs were clustered into different Nb-

791 Sets. Overall, five Nb-Sets were identified. Set 1: NM1228, NM1226, NM1227, NM1229; Set

792 2: NM1230, NM1221, NM1222, Set 3: NM1223; Set 4: NM1224; Set 5: NM1220.

793

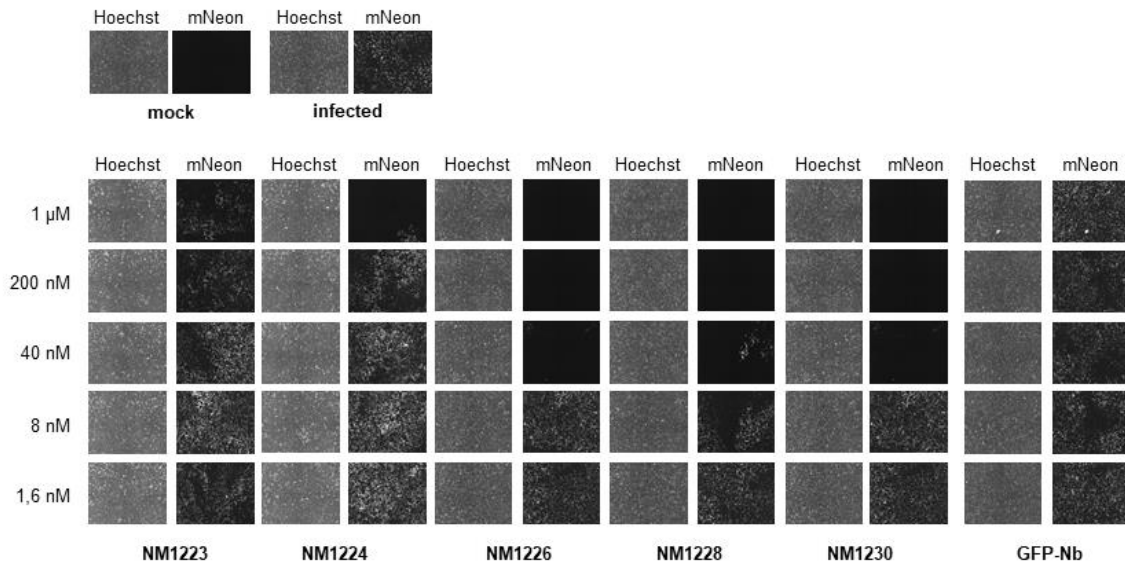


794

795 **Supplementary Figure 3 Epitope mapping of Nbs by HDX mass spectrometry**

796 Surface structure fge model of the RBD domain showing the ACE2 interface and the HDX-MS
 797 epitope mapping results of Nb-Set2. Residues of the RBD (PDB 6M17 [2]) responsible for
 798 contact of the ACE2 [2, 35] are shown in red (top panel). RBD epitopes protected upon binding
 799 of NM1221, NM1222 and NM1230 are highlighted.

800

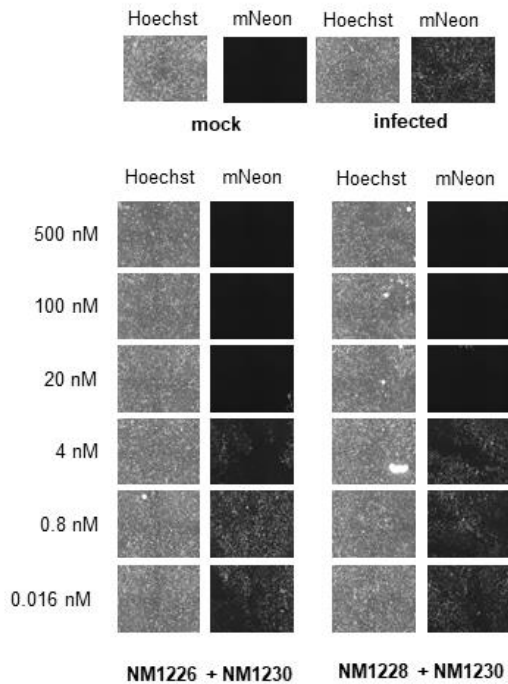


801

802 **Supplementary Figure 4: Viral neutralization potency of selected Nbs**

803 Inhibition of viral infectivity of the SARS-CoV-2 strain icSARS-CoV-2-mNG was analyzed in
804 Caco-2 cells using serial dilutions of NM1223, NM1224, NM1226, NM1228 and NM1230. As
805 negative control the GFP-Nb was used. 48 h post-infection neutralization potency was
806 visualized via Hoechst staining and mNeonGreen expression. Representative images of
807 human Caco-cells upon infection with SARS-CoV-2 expressing mNeonGreen (icSARS-CoV-
808 2-mNG) either in presence or absence of serial dilutions of RBD Nbs are shown.

809

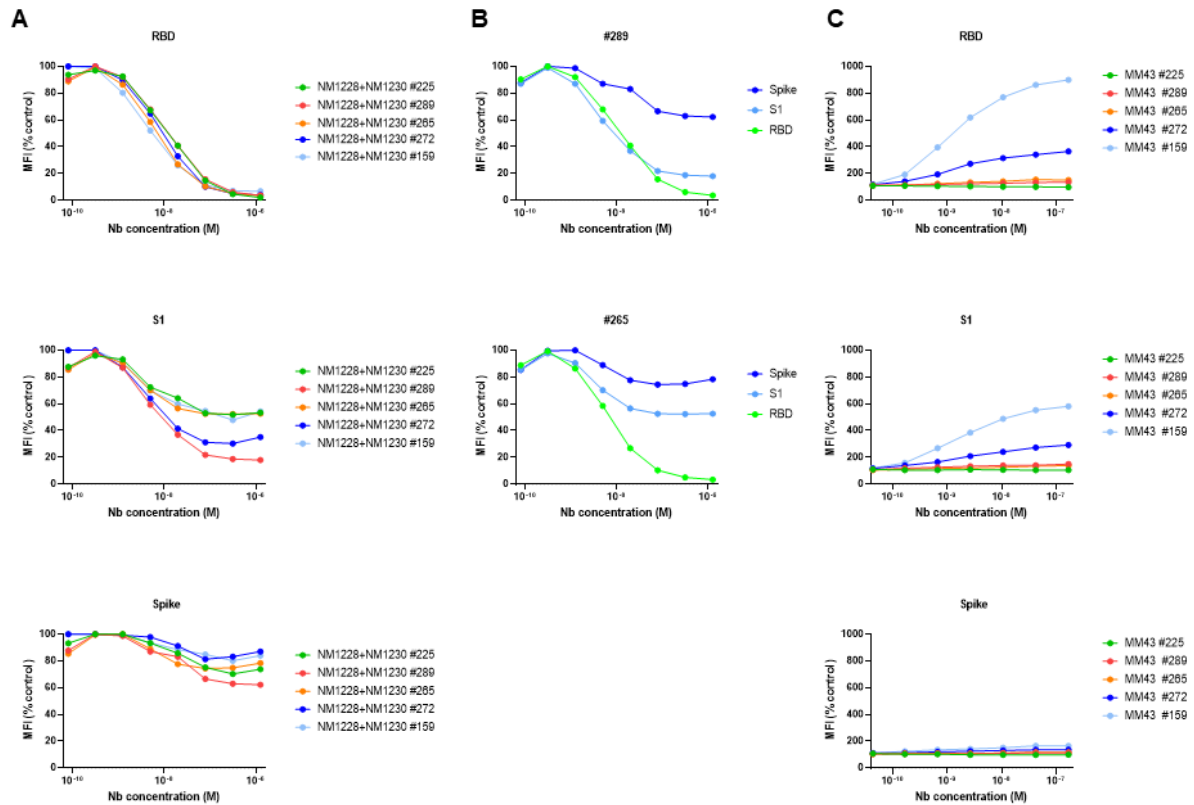


810

811 **Supplementary Figure 5: Viral neutralization with Nb combinations**

812 Inhibition of viral infectivity of the SARS-CoV-2 strain icSARS-CoV-2-mNG was analyzed in
813 Caco-2 cells using serial dilutions of Nb combinations NM1226/ NM1230 and NM1228/
814 NM1230. 48 h post-infection neutralization potency was visualized via Hoechst staining and
815 mNeonGreen expression. Representative images of human Caco-cells upon infection with
816 SARS-CoV-2 expressing mNeonGreen (icSARS-CoV-2-mNG) either in presence or absence
817 of serial dilutions of combinations of RBD Nbs are shown.

818

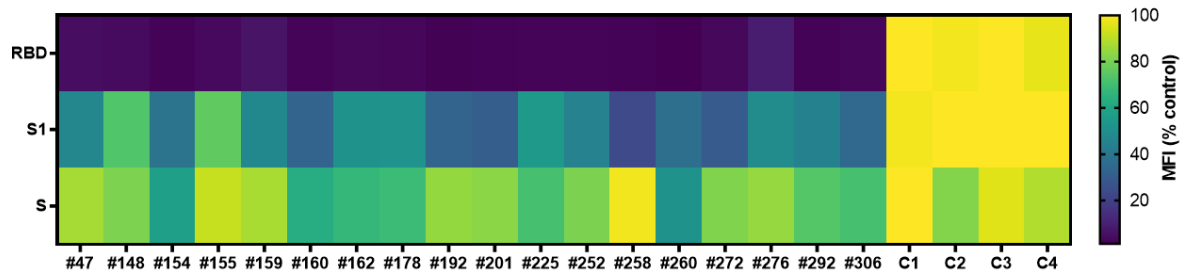


819

820 **Supplementary Figure 6: The NeurobodyPlex - multiplex competitive binding assay to**
821 **monitor a neutralizing immune response in patients**

822 **(A)** For the NeurobodyPlex assay serial dilutions (1.26 μ M to 7.69 pM per Nb) of the
823 combination NM1228/ NM1230 were incubated with five serum samples followed by detection
824 of bound human IgGs. Shown are MFI signals obtained for all three Spike-derived antigens
825 normalized to serum-only control. **(B)** For two serum samples (#289, #265) differences in Nb
826 competition efficiency between the three Spike based antigens are shown. **(C)** Curves as
827 presented, show normalized MFI signals derived from a similar assay using the neutralizing
828 mouse antibody MM43 in concentrations ranging from of 0.17 μ M to 0.08 nM instead of Nb
829 combinations.

830



831

832 **Supplementary Figure 7: NeutrobodyPlex validation by testing of patient samples**

833 18 serum samples from SARS-CoV-2 convalescent patients and four from healthy donors (C1-
834 4) were analyzed using the NeutrobodyPlex using a fixed concentration of the Nb combination
835 NM1228/ NM1230 (1.26 μ M per Nb). MFI values normalized to serum only control are
836 illustrated as heat map graphic. Dark blue color coding represents loss of the detectable signal,
837 meaning a strong shift of serum antibodies into the unbound state by off-competition of Nbs.
838 Yellow color coding represents no signal differences in presence or absence of Nbs.

839

